Highly Efficient Quasi-Solid-State Asymmetric Supercapacitors Based on MoS$_2$/MWCNT and PANI/MWCNT Composite Electrodes

Bing Cheng[1,2], Renzhi Cheng[1,2], Furui Tan[1,2], Xiansheng Liu[1,2], Jinghao Huo[3] and Gentian Yue[1,2*]

Abstract

Molybdenum disulfide (MoS$_2$) and polyaniline (PANI) electrodes were decorated with multi-walled carbon nanotubes (MWCNTs) on the basis of a facial hydrothermal and in situ polymerization methods and served in the asymmetric supercapacitor (ASC). The MoS$_2$ and MWCNTs with a mole ratio of 1:1 in MoS$_2$|MWCNTs electrode exhibited better electrochemical properties through extensive electrochemical studies, in terms of the highest specific capacitance of 255.8 F/g at 1 A/g, low internal resistance, and notable electrochemical stability with retention of the initial specific capacitance at 91.6% after 1000 cycles. The as-prepared PANI|MWCNTs electrode also exhibited good specific capacitance of 267.5 F/g at 1 A/g and remained 97.9% capacitance retention after 1000 cycles. Then, the ASC with MoS$_2$|MWCNTs and PANI|MWCNTs composite electrodes were assembled with polyvinyl alcohol (PVA)-Na$_2$SO$_4$ gel electrolyte, which displayed good electrochemical performance with the specific capacitance of 138.1 F/g at 1 A/g, and remained the energy density of 15.09 Wh/kg at a high power density of 2217.95 W/kg. This result shows that this ASC device possesses excellent electrochemical properties of high energy density and power output and thus showing a potential application prospect.

Keywords: Molybdenum disulfide, Multi-walled carbon nanotube, Polyaniline, Quasi-solid-state, Supercapacitor

Background

With the energy crisis and environmental pollution increasing seriously, the efficient and stable energy storage equipment has attracted extensive research due to the intermittent energy sources (such as solar energy, wind power, and frictional power) cannot continuously and stably output electrical energy for daily application [1, 2]. Supercapacitors (SCs) with fast charging/discharging and long cycling life are considered as an ideal choice for energy storage devices, which overall performance is mainly determined by the most important components, i.e., electrode materials [3]. Typically, a significant amount of electrode materials, like graphene, carbon nanotubes (CNTs), conducting polymers, and oxide metals, have become a

research focus [4–7]. In particular, pseudocapacitive materials with remarkably high capacitance have attracted a large number of concerns [8].

Among these reports, carbon materials are identified as one of the most popular because of their excellent conductivity, large surface area, environmental friendly protecting, and low cost. However, the carbon materials store charges by electric double-layer capacitor mechanism possess high electrical conductivity but low capacitance. Thus, to improve the electrochemical performance of carbon-based materials, researchers have devoted great efforts to grow nano-structured active materials on them [9–15]. Molybdenum disulfide (MoS$_2$), as a typical family member of transition-metal dichalcogenides (TMDs), has attracted lots of attention for its special structural and chemical character, which is extensively applied in many fields including lithium-ion batteries, catalysis, and dye-sensitized solar cells. MoS$_2$ with nanoscale recently has been chosen to use in capacitors

* Correspondence: yuegentian@126.com; zhenghaiwu@ustc.edu
[1]Henan Key Laboratory of Photovoltaic Materials and Laboratory of Low-Dimensional Materials Science, Henan University, Kaifeng 475004, China
[2]School of Physics and Electronics, Henan University, Kaifeng 475004, China
Full list of author information is available at the end of the article

Cheng *et al. Nanoscale Research Letters* (2019) 14:66

Page 2 of 12

owing to its higher intrinsic fast ionic conductivity than oxides and higher theoretical capacity than graphite besides high surface area. Wang et al. [16] prepared MoS_2 with hierarchical hollow nanospheres structure as negative electrode material providing a maximum specific capacitance of 142 F/g at 0.59 A/g. Yang et al. [17] designed MoS_2/graphene nanosheet composites and obtained a specific capacitance of 320 F/g at 2 A/g. Hu et al. [18] prepared porous $C|MoS_2$ electrode which obtained the specific capacity of 210 F/g at 1 A/g and good stability with more than 1000 cycles at 4 A/g. However, the poor specific capacitance of MoS_2 attributed to the stacking and collapse in the charge-discharge process of its two-dimensional layered structures, which limits the application in SCs. Therefore, how to construct hierarchical three-dimensional (3D) architectures is an effective way to solve the problem of aggregation and prepare high-performance supercapacitors based on MoS_2 composites electrode.

In addition, with reported good conductivity, ease of synthesis, low-cost monomer, tunable properties, and remarkable specific capacitance (500–2200 F/g), polyaniline (PANI) has been extensively studied as a pseudo-supercapacitor electrode material [19–21]. Recently, many researchers have combined PANI with carbon materials and transition metal compound to improve the conductivity of the PANI-based electrodes for enhancing the cycling stability and rate capability of the PANI-based pseudo-super-capacitors [22–27]. For example, Li and his workers [28] prepared 3D CNTs|PANI fibers and obtained a specific capacitance as high as 242.9 F/cm in 1 M H_2SO_4 electrolyte. Das et al. [29] reported an asymmetric supercapacitor (ASC) assembled with a Prussian blue/MnO_2-positive electrode and a PANI/graphene nanoplatelet composite as the negative electrode in KNO_3 electrolyte and exhibited manifested favorable specific capacitance of 98 F/g at 1 A/g. Ghosh et al. [30] have fabricated high-energy density all-solid-state flexible ASC by using a facile novel 3D hollow urchin-shaped coaxial MnO_2@PANI composite as positive electrode and 3D graphene foam as negative electrode materials with polyvinyl alcohol (PVA)/KOH gel electrolyte. Conductive PANI not only works as the bridge between MnO_2 and graphene to enhance the electrical conductivity, but also improves the specific capacitance of the electrode. Moreover, recent studies also exhibited that gel electrolyte has revealed the most potential application prospects for supercapacitors [31, 32].

In view of these, we prepared MoS_2 bridged by multi-walled carbon nanotubes (MWCNTs) through a facile hydrothermal method and prepared the PANI decorated with MWCNTs composite by using in situ chemical polymerization process. After extensive electrochemical testing, the specific capacity of $MoS_2|MWCNTs$ and PANI|MWCNTs electrodes

obtained 255.8 F/g and 267.5 F/g at 1 A/g, respectively. The retention rate of the $MoS_2|MWCNTs$ electrode retained 91.6% after 1000 cycles at the scan rate of 30 mV/s. Also, the PANI|MWCNTs electrode also exhibited 97.9% retention at the scan rate of 60 mV/s after 1000 cycles. A quasi-solid-state ASC based on $MoS_2|MWCNTs$ and PANI|MWCNTs electrodes with PVA-sodium sulfate (Na_2SO_4) gel electrolyte showed energy density of 38.9 Wh/kg at the power density of 382.61 W/kg. Two such super quasi-solid-state ASC in series can easily light a red light-emitting diode, indicating potential application prospects.

Methods

Synthesis of $MoS_2|MWCNTs$

The preparation of MoS_2 is done by using a simple hydrothermal method [33]. Firstly, 0.726 g of sodium molybdate and 0.684 g of thiourea were mixed together in 35 ml of deionized water by stirring and sonicating for 30 min successively. Then, a certain amount of MWCNTs with different contents was added into the above mixture and sonicated for another 30 min. Subsequently, the mixed solution was adjusted the PH to less than 1 with 12 M hydrochloric acid. After that, the solution was transferred into a 50-ml Teflon liner and heated at 200 °C for 24 h without intentional control of ramping or cooling rate. When the temperature cooled down to room temperature, the precipitation was collected by filter and washed with ethanol and distilled water for five times, and then dried in a vacuum oven at 60 °C for 24 h. Furthermore, the mole ratios of MoS_2 and MWCNTs with 2:1, 1:1, and 1:2 were also researched and labeled as MS2MWCNT1, MS1MWCNT1, and MS1MWCNT2 respectively. For comparison, pure MoS_2 and MWCNTs were labeled as MS1MWCNT0 and MS0MWCNT1, respectively.

Synthesis of PANI|MWCNTs

The preparation of PANI|MWCNTs was based on the previous reported [34, 35]. Firstly, 18 mg of MWCNTs were dispersed in 10 ml of deionized water and sonicated for 0.5 h and labeled as solution A. Then, 0.3 ml of aniline monomer was dissolved in 10 ml of 1 M hydrochloric acid and labeled as solution B. Subsequently, 0.21 g of potassium persulfate was dissolved in 10 ml of 1 M hydrochloric acid and labeled as solution C. Afterwards, solution B was added to solution A under magnetic stirring followed by sequential addition of solution C drop by drop, until the mixed solution turned dark green. At room temperature, this reaction continued for more than 5 h. After that, the product was collected by centrifugation and washed repeatedly with deionized water and absolute ethanol. The as-prepared sample was labeled as PANI|MWCNTs.

Cheng *et al. Nanoscale Research Letters* (2019) 14:66

Page 3 of 12

Preparation of Quasi-Solid-State ASC

The quasi-solid-state ASC assembled as a sandwich structure by clipping a MoS₂|MWCNTs cathode and a PANI|MWCNTs anode with PVA-Na₂SO₄ quasi-solid-state electrolyte, and the ASCs were labeled as MoS₂|MWCNTs//PANI|MWCNTs (MM//PM). Firstly, the electrode material slurry as the mass ratio of active material (MoS₂|MWCNTs and PANI|MWCNTs composites), nano graphite powder, and PVDF is 75:15:10 in NMP solvent, which was loaded on foam nickel to be pressed by using a doctor blade method. Prior to testing, the electrode material was dried in a vacuum oven at 60 °C for 12 h, and then immersed in the 0.5 M Na₂SO₄ electrolyte for 12 h. To prepare the PVA-Na₂SO₄ gel, 2 g of PVA was dissolved in deionized water at 90 °C and then 0.5 M Na₂SO₄ was added under vigorous stirring to obtain a clear solution. The gel was allowed to cool to room temperature after which it was used to fabricate the ASC.

Characterization and Electrochemical Measurement

The surface morphologies of the samples were observed by using JSM-7001F field emission scanning electron microscope (SEM). The crystalline structures of the composites were investigated by glancing incident X-ray diffractometer (X'Pert Pro, PANalytical B.V., Netherlands). Raman scattering was collected on a Renishaw RW1000 confocal microscope with 514 nm line of Ar + iron laser as the exciting light.

Cyclic voltammetry (CV) measurements were conducted in a three-electrode one-compartment cell, in which an as-prepared sample electrode was taken as the working electrode, a Pt sheet of 1.5 cm² as CE, and an Ag/AgCl electrode as a reference electrode in 6 M aqueous KOH solution. The electrochemical impendence spectroscopy (EIS) tests were carried out simulating open-circuit conditions at ambient atmosphere by using an electrochemical measurement system (CHI660E, Shanghai Chenhua Device Company, China) at a constant temperature of 20 °C with AC signal amplitude of 20 mV in the frequency range from 0.1 to 10^5 Hz at 0 V DC bias in the dark. The galvanostatic current charge-discharge (GCD) curves were conducted using a computer-controlled electrochemical analyzer (CHI 660E, CH Instrument). The specific capacitance (Cs) of the supercapacitor was calculated according to the following equations [36–39]:

$$C_s = \frac{4 \times \Delta t}{\Delta V \times m_{ac}} \tag{1}$$

where I represents the current density (A), Δt represents the discharge time (s), ΔV represents the working potential window (V), m_{ac} represents the quality of active materials (g).

Results and Discussion

Cathode Material: MoS₂|MWCNTs

Figure 1 shows the SEM images of the MoS₂ and MS1MWCNT1 composite. From Fig. 1a and Fig. 1b, it can be seen that the synthesis of MoS₂ nanospheres with honeycomb structure has a uniform distribution and similar particle size. From Fig. 1b, it exhibits that the surface of MoS₂ nanospheres has many wrinkles, which
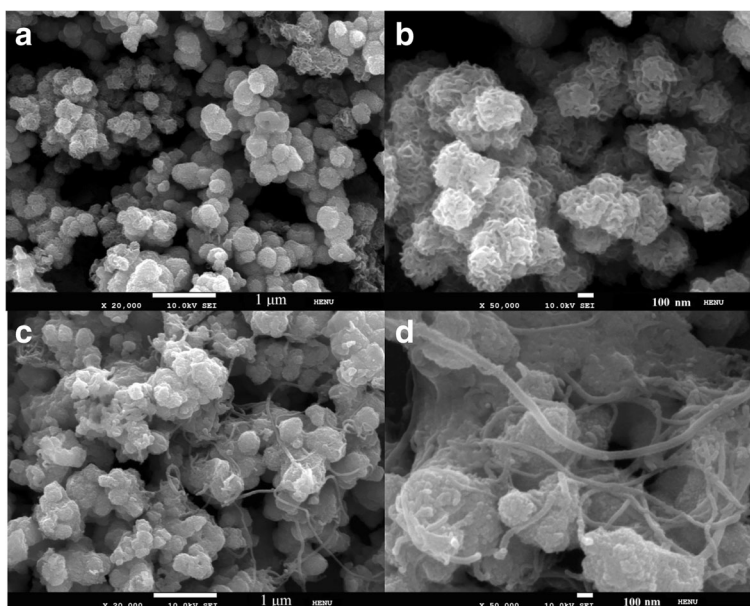

Fig. 1 The SEM images of the MoS₂ nanospheres (**a**, **b**) and the composite of MS1MWCNT1 (**c**, **d**)

are due to the stacking of the MoS_2 nanosheets resulting in agglomerated spheres. Such a structure not only helps to provide large specific surface area, but also contributes to the diffusion and transfer of ions. Figure 1c and Fig. 1d show the images of MS1MWCNT1 composite, in which the MoS_2 nanoclusters are bridged together by MWCNTs and form the MS1MWCNT1 composite. The MWCNTs have good conductivity and large specific surface area, which can compensate for the poor conductivity of MoS_2 and provide more active sites by the edge of MWCNTs.

The structural characteristics of the as-prepared MoS_2, MWCNTs, and MS1MWCNT1 were exhibited by Raman spectrum and XRD patterns. From Fig. 2a, there are two strong and sharp peaks at 375 and 408 cm^{-1} for MoS_2. The former characteristic peak is called the E_{2g} mode due to the in-plane vibration of the two S atoms relative to the Mo atom in the opposite direction. The latter characteristic peak is called the A_{1g} mode for the non-plane S atom vibration in the opposite direction [40, 41]. For the Raman characteristic peaks of MWCNTs, the D and G peaks are around 1350 and 1580 cm^{-1}, respectively [42, 43]. From these peaks ratios, we can see that the MWCNTs have good crystal purity and defect density. For the MS1MWCNT1 composite, the characteristic peaks of MoS_2 and MWCNTs all exist and there are no new peaks emerge except a little red shift. The phenomenon of a little red shift for the MS1MWCNT1 composite can be responsible for the change of particle size and pore diameter. On the whole, this result indicates that the MS1MWCNT1 is successfully prepared without new compound formation.

Figure 2b shows XRD patterns of MoS_2, MWCNTs, and MS1MWCNT1 samples. The diffraction peaks at 14.46°, 33.28°, and 58.66° are the contributions of MoS_2 [44].9 Among them, the absence of strong diffraction peak of MoS_2 reveals that stacking of the single layers very possibly takes place, which is named graphene-like structure. The diffraction peaks at 26.09° and 43.44° correspond to the signals of MWCNTs [45]. As for the XRD patterns of the MS1MWCNT1 composite, it exhibits all the characteristics of diffraction peaks for the MWCNT and MoS_2. Especially, the strong peak at 14.46° of the MoS_2 manifests a well-stacked layered structure, which demonstrates that the crystallinity of MoS_2 is greatly improved after recombination. The Raman and XRD results indicate that the MoS_2 and MWCNTs composite are synthesized successfully.

The electrochemical characteristics of the as-prepared MoS_2|MWCNTs electrodes are measured by CV, GCD, and EIS tests in Fig. 3. Figure 3a shows the CV curves for the MoS_2|MWCNTs electrodes with different mole ratios of MoS_2 and MWCNTs at 20 mV/s. The integrated CV area of the MoS_2|MWCNTs electrodes shows larger than the pristine MWCNT and MoS_2 electrodes, indicating the capacitance improvement for the synergistic effect from the excellent conductivity of MWCNTs and the high electrochemical performance of MoS_2. Similarly, the MS1MWCNT1 electrode presents the largest CV area than that of the MS1MWCNT2 and MS2MWCNT1 electrodes, indicating excellent pseudocapacitive behavior for the MS1MWCNT1 electrode. In addition, the CV curves of the MS1MWCNT1 electrode with different scan rates ranging from 5 to 50 mV/s are tested as shown in Fig. 3b. As we can see from the curves, the current density and redox peaks increase regularly with the enlargement of scan rate, suggesting an excellent rate
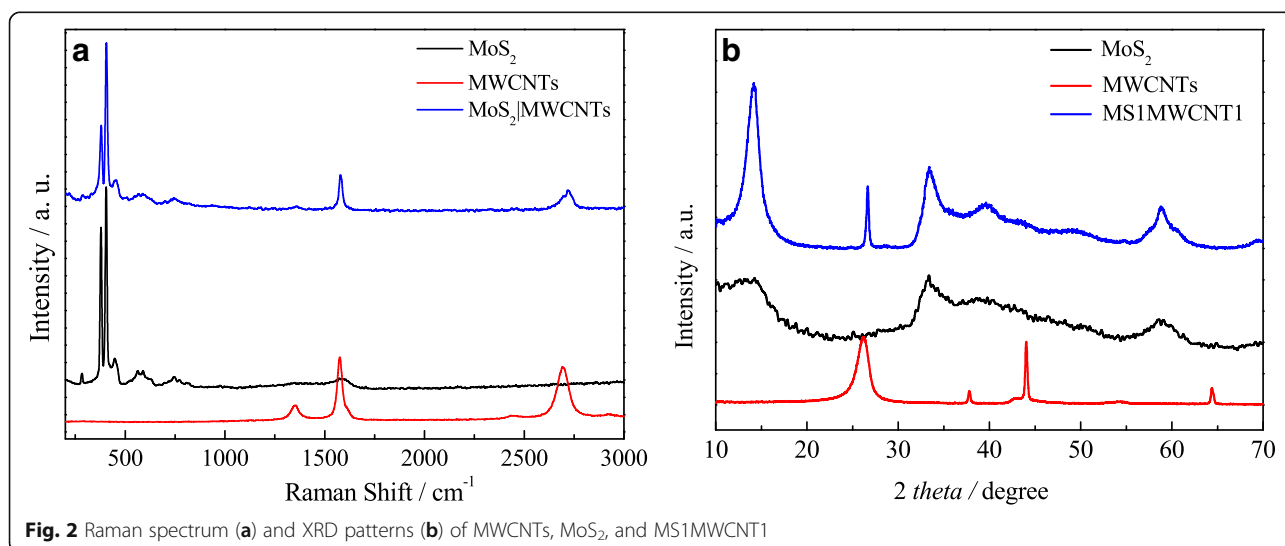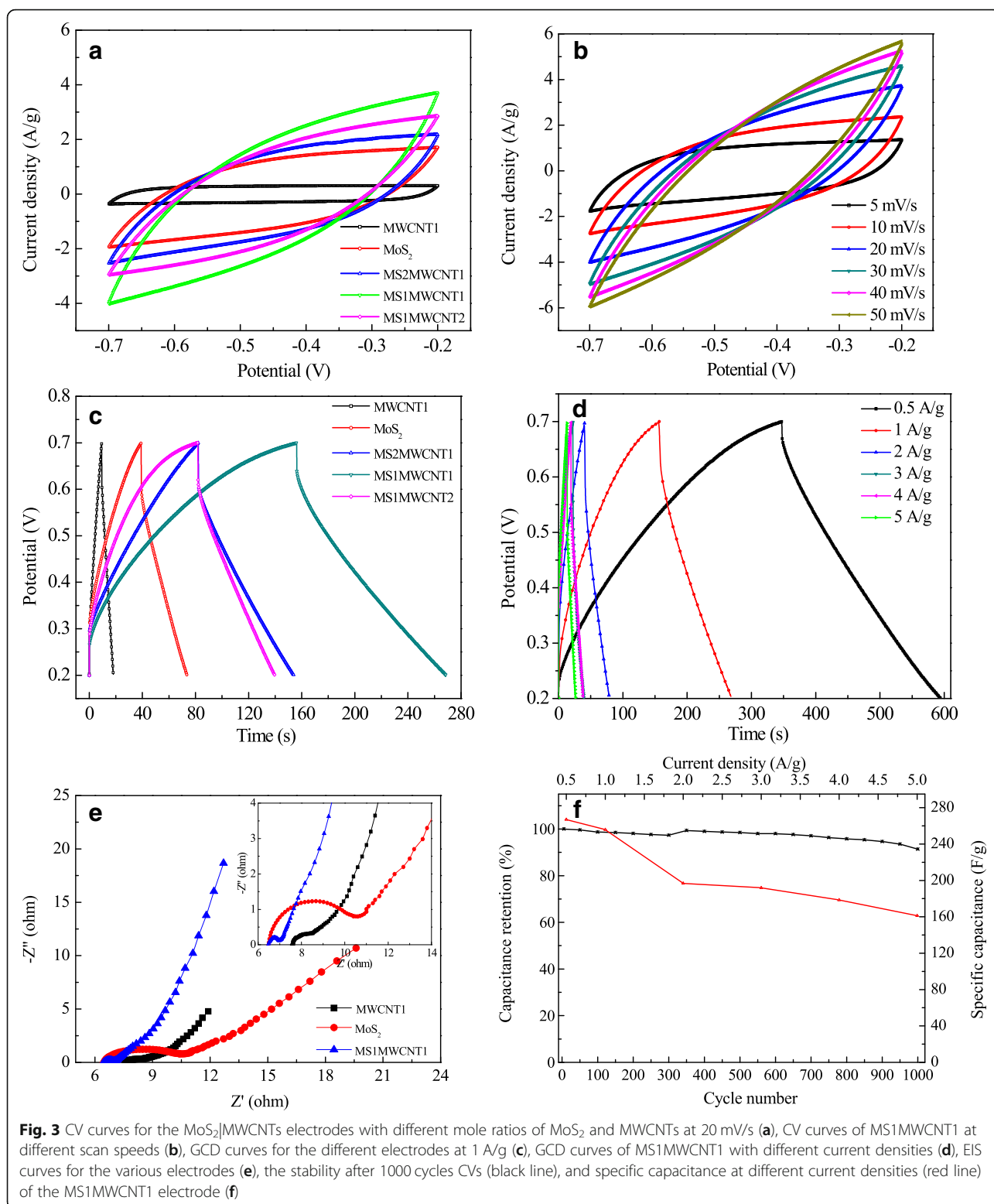

Fig. 2 Raman spectrum (**a**) and XRD patterns (**b**) of MWCNTs, MoS_2, and MS1MWCNT1

Fig. 3 CV curves for the MoS$_2$|MWCNTs electrodes with different mole ratios of MoS$_2$ and MWCNTs at 20 mV/s (**a**), CV curves of MS1MWCNT1 at different scan speeds (**b**), GCD curves for the different electrodes at 1 A/g (**c**), GCD curves of MS1MWCNT1 with different current densities (**d**), EIS curves for the various electrodes (**e**), the stability after 1000 cycles CVs (black line), and specific capacitance at different current densities (red line) of the MS1MWCNT1 electrode (**f**)

capability and good reversibility of redox procedure [46, 47]. Figure 3c shows GCD curves for the different electrodes at 1 A/g. According to Fig. 3c, the pure MWCNTs and MoS$_2$ electrodes get specific

capacitances of 30.4 and 90.6 F/g at 1 A/g, which are smaller than that of the MoS$_2$|MWCNTs electrode. It is very interesting that the specific capacitance has increased obviously when MoS$_2$ is decorated with

MWCNTs. This is attributed to the good combination of conductive MWCNTs and MoS_2 with high ionic conductivity, and the using of MWCNTs as a skeleton helps to increase the mechanical stability of the composite to prevent damage from electrical factors during charging and discharging. When the content of MWCNTs is small, the specific capacitance of MS2MWCNT1 is 132.4 F/g. With the MWCNTs percentage increasing and the mole ratio of MoS_2 and MWCNTs reaches 1:1 in the composite materials, the specific capacitance gets 255.8 F/g at 1 A/g, which is much higher than that of the MS2MWCNT1 electrode. While the mole ratio of MoS_2 and MWCNTs is beyond 1:1, the specific capacitance of the MS1MWCNT2 electrode begins to decrease and achieves a much smaller specific capacitance of 173.4 F/g at 1 A/g, which can be due to the small capacity of the MWCNTs. Figure 3d presents the GCD curves for the MS1MWCNT1 electrode at various current densities (0.5, 1, 2, 3, 4, and 5 A/g), which shows the specific capacitance decreases with increasing of the current density. This is because the diffusion and transfer of ions are limited at higher current density, and the lower current density can reduce the probability of destruction of the electrode material by the large electric field, so that the effective storage of charges decreases with the current density increasing. Also, the GDC curve of the MS1MWCNT1 electrode maintains a negligible voltage drop during the charging and discharging process, indicating the pseudocapacitive contribution along with the double layer contribution. The specific capacitance of MS1MWCNT1 electrode reaches 266.9 F/g at 0.5 A/g. The excellent energy storage characteristic is responsible for the large surface area and the high electrical conductivity, which provides additional electrochemical active sites and short paths for rapid ion diffusion and transport. As the current density increases to 5 A/g, the specific capacitance of MS1MWCNT1 electrode remains 203.5 F/g, demonstrating a good rate capability for the electrode. Figure 3e shows the EIS of the MoS_2, MWCNTs, and MS1MWCNT1 electrodes to understand the impedance behavior. The enlarge EIS figure is shown as the inset. The diameter of the depressed semicircle of the Nyquist plots quantifies the charge-transfer resistance (Rct) at the electrode|electrolyte interface [48], which are found to be 4.11, 1.36, and 0.59 Ω for the MoS_2, MWCNTs, and MS1MWCNT1 electrodes, respectively. The MS1MWCNT1 electrode shows the lowest Rct value compared to the MoS_2 and MWCNTs electrodes, indicating that the EIS improvement for the synergistic effect of MWCNTs and MoS_2 is helpful to decrease the energy loss at high power output. Moreover, the Warburg resistance (Wd) indicates the ionic diffusion/transport from the electrolyte to the surface of the electrode [48]. From Fig. 3e, the MS1MWCNT1 electrode exhibits a more vertical line comparing with the MoS_2 and MWCNTs electrodes at low frequencies, which is explained that the MS1MWCNT1 electrode has a larger specific surface area, thus providing greater contact area for the electrode materials and electrolyte and helping to absorb more electrolyte [49]. Figure 3f shows the cycle stability (black line) and specific capacitance at different current densities (red line) of the MS1MWCNT1 electrode after 1000 cycles (extract a loop every 50 laps). From the black line, a small increase of capacitance is observed during the first 350 cycles, and the capacitance still maintains about 91.6% of the initial capacitance after 1000 cycles, indicating good cycling life of the composite materials [50]. The initial increase of capacitance can be attributed to gradual wetting of the electrolyte deep inside the electrode material. Then, the electrochemical active Mo sites inside the substrate electrode will be fully exposed

Table 1 A comparison of the characteristics of various MoS_2 or PANI for supercapacitors

Electrode materials	Electrolyte	Specific capacitances	Capacity retention rates	Ref.
CNTs|MoS_2	1 M Na_2SO_4	74.05 F/g at 2 A/g	81% after 1000 cycles	[56]
Tubular C|MoS_2	3 M KOH	210 F/g at 1 A/g	105% after 1000 cycles	[18]
CNTs|PANI	1 M H_2SO_4	113.64 F/cm^2 at 1 mA	90.2% after 1000 bending cycles	[28]
MoS_2|rGO|Ti mesh	PVA-1 M NaCl	17.6 mF/cm^2 at 10 mV/s	–	[35]
MoS_2|Mo	1 M Na_2SO_4	192.7 F/g at 1 mA/cm^2	98% after 1000 cycles	[54]
MoS_2|SiO_2	2 M KOH	683 F/g at 1 A/g	85% after 10,000 cycles	[39]
MoS_2 nanosheets	1 M Na_2SO_4	129.2 F/g at 1 A/g	85% after 500 cycles	[40]
1D PANI|2D MoS_2	1 M Na_2SO_4	485 F/g at 1 mA/cm^2	–	[51]
MS1MWCN1	0.5 M Na_2SO_4	255.8 F/g at 1 A/g	95.02% after 500 cycles	This work
PANI|MWCNTs	0.5 M Na_2SO_4	267.49 F/g at 1 A/g	94.5% after 500 cycles	This work
Quasi-solid-state MM//PM	PVA-Na_2SO_4	138.13 F/g at 1 A/g	–	This work

to the electrolyte. Therefore, an increasing capacitance is displayed in the cyclic tests. Compared with other MoS$_2$/carbon-based composites (Table 1), the MS1MWCNT1 electrode displays higher specific capacitance and more excellent electrochemical stability. Furthermore, the obtained maximum specific capacity is 266.9 F/g corresponding to the current density of 0.5 A/g for the MS1MWCNT1 electrode. When the discharge current density is further increased, the specific capacity decreases slowly, and 161.3 F/g is observed at 5 A/g. This is responsible for the resistance of the electrode and the insufficient Faradaic redox reaction of the active material under higher discharge current density.

Anode Material: PANI|MWCNTs Composite Materials

Figure 4 shows the SEM images of the PANI|MWCNTs. Figure 4b is the enlarge figure from Fig. 4a. From the SEM images, it can be seen that the PANI coats on MWCNTs surface and forms a perfect organic-inorganic composite material. The MWCNTs framework helps to increase the mechanical stability of PANI and the diffusion of ions and also contributes to the improvement of the conductivity of PANI. Moreover, the pseudo-capacitance of PANI is a benefit to increase the specific capacitance of the PANI|MWCNTs composite material.

Figure 5 shows several Raman peaks for the structural features of MWCNTs, PANI, and PANI|MWCNTs. Among them, Raman peaks at 1165, 1308–1347, 1468, and 1593 cm^{-1} are the characteristic peaks of PANI [51]. In the PANI|MWCNTs composite material, the characteristic peaks of PANI and MWCNTs (we have discussed in Fig. 2) are all observed though the peak signal of from MWCNT is not obvious, which is responsible for the low contents of MWCNTs and strong signals of PANI. To sum up, this result indicates that the PANI is well wrapped on the surface of the MWCNTs.

Figure 6a shows the GCD curves of PANI, MWCNTs, and PANI|MWCNTs electrodes at 1 A/g. From Fig. 6a, it can be seen that the voltage window of the PANI|MWCNTs electrode is much higher than that of the pure PANI or MWCNTs electrode. This may be related to the conductivity of the pure PANI and MWCNTs. This result clearly shows the improvement in voltage window for the pseudocapacitors with the MWCNTs-based composites [52]. Figure 6b shows the CV curves of PANI|MWCNTs electrode at different scanning speeds, showing the capacitive behavior of PANI|MWCNTs electrode can be greatly improved by loading of PANI. Figure 6c illustrates GCD curves of PANI|MWCNTs electrode at different current densities of 0.5, 1, 2, 3, 4, and 5 A/g, and the corresponding specific capacitance is observed to be 258.4, 267.5, 218.9, 192.8, 173.7, and 150.8 F/g, respectively, which can be calculated from Eq. (1). It shows that the discharge time is short at high current density whereas lower current density resulted in a longer discharge time. The reason why is that the slower charge-discharge rate enables the ions to have enough time for accessing the electroactive sites which are not available at higher current densities due to the time constraints of the electrolyte ions [53, 54]. In Fig. 6d, it can be seen that the Rct of the PANI|MWCNTs electrode decreases as expected compared to that of the PANI and MWCNTs electrodes. At the same time, the slope of the EIS plot for the PANI|MWCNTs electrode is steeper than that of the PANI or MWCNTs electrode in the low-frequency region. These results indicate that the PANI|MWCNTs electrode has better capacitance performance. Figure 6e shows the cycle stability (black line) and specific capacitance at different current densities (red line) of PANI|MWCNTs electrode. From the curves, it exhibits a small increase of capacitance during the first 150 cycles and remains 97.9% capacitance retention after 1000 cycles, indicating a preferable long-term cycling stability. This is because the PANI and MWCNTs nanowires can effectively increase the stability for the electrode material [55]. The red line shows the change of the specific capacity for the
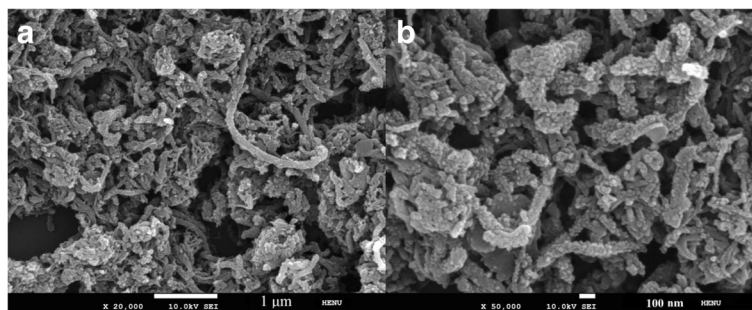

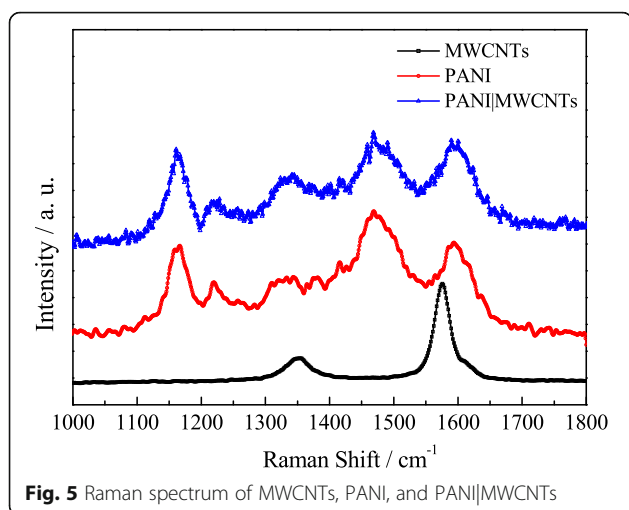**Fig. 4** The SEM images of the PANI|MWCNTs (**a**, **b**)

Fig. 5 Raman spectrum of MWCNTs, PANI, and PANI|MWCNTs

PANI|MWCNTs with the changing of current density. On the whole, the specific capacity decreases with the increasing current density can be attributed to the same reasons as MS1MWCNT1 electrode. Very interestingly, the specific capacity of PANI|MWCNT hybrids increases at 1.0 A/g and then decreases. This may be due to the electrode material being further activated during charging and discharging, or the electrolyte ions cannot enter certain sites of electrode materials at low current density.

Quasi-Solid-State ASC: MM//PM

Figure 7a shows that the voltage window of as-assembled quasi-solid-state MM//PM ASC can be expanded to 1.5 V. As expected, the CV curves of the as-assembled ASC can retain the quasi-rectangular shape even at 1.5 V. These quasi-rectangular curves support the quasi-solid-state MM//PM ASC with excellent capacitive behavior and reversible charging-discharging process. In order to further measure the electrochemical performance, the quasi-symmetrical shape between the discharge and charge curves ranging from 0.5 to 4 A/g were carried out and are shown in Fig. 7b, indicating that the MM//PM ASC demonstrates a good capacitive behavior with high columbic efficiency. Figure 7c shows the typical Nyquist plots for quasi-solid-state MM//PM ASC, including the solution resistance (Rs) of 20.86 Ω and charge transfer resistance (Rct) of 15.49 Ω. The low EIS of MM//PM ASC can be attributed to the introduction of MWCNTs, which results in mitigating the agglomeration of the MoS_2 and enhancing electrical conductivity, and a conductive network connected by carbon nanotubes is beneficial to the transportation of ions and charges at the interface of electrode|electrolyte. At low frequencies, a line with a steep slope appears, indicating that MM//PM ASC has a superior capacitance behavior, which is due to the synergistic effect of double

electric layer characteristics and pseudo-capacitance characteristics came from MWCNTs, PANI, and the high wettability and good catalytic of the MoS_2. The black line in Fig. 7d shows the cycle stability of the MM//PM ASC, which also exhibits a small increase of capacitance at the initial 100 cycles and then shows a gentle downward trend and remains 65.2% capacitance retention after 1000 cycles, indicating a preferable long-term cycling stability with gel electrolyte for the MM//PM ASC. This is because the carbon nanotube skeletons and the gel electrolyte can effectively improve the stability for the MM//PM ASC. The red line in Fig. 7d exhibits the specific capacitance of the MM//PM ASC with different charging current densities. The specific capacitance decreases with the increasing of current density, indicating less active material access and reducing the effective utilization of material at a higher scan rate [20]. Among them, the maximum specific capacitance of 138.13 F/g is observed for the quasi-solid-state MM//PM ASC at 1 A/g.

The Ragone plot of the as-prepared quasi-solid-state MM//PM ASC is shown in Fig. 8a. The energy and power densities are derived from GCD at different current densities. From the Ragone plots, the quasi-solid-state MM//PM ASC shows a high energy density of 38.9 Wh/kg at a power density of 382.61 W/kg. Even at a high-power density of 2217.95 W/kg, a relatively high energy density of 15.09 Wh/kg still remains. The results illustrate that the quasi-solid-state MM//PM ASC has excellent electrochemical properties of high energy density and power output. In order to demonstrate the actual output power, Fig. 8b shows that the red LED bulb can be easily lighted based on a series group consisted of two neutral quasi-solid-state MM//PM ASCs, suggesting the potential application.

Conclusion

In summary, two composites of MoS_2- and PANI-mixed MWCNTs are prepared by using simple hydrothermal and low-cost chemical polymerization method and served as cathode and anode electrode' materials for asymmetric supercapacitor devices. The specific capacitances of MS1MWCNT1 and PANI|MWCNTs electrodes are 255.8 and 267.5 F/g at 1 A/g, respectively through extensive electrochemical testing. These active composite materials not only maintain the higher stability and conductivity, but also have a larger capacity than that of a single one, which implies that the composite materials produce a better specific capacitance, higher energy, and power densities for their synergistic effect. Besides, the quasi-solid-state MM//PM ASC based on PVA-Na_2SO_4 gel electrolyte exhibits a good charge
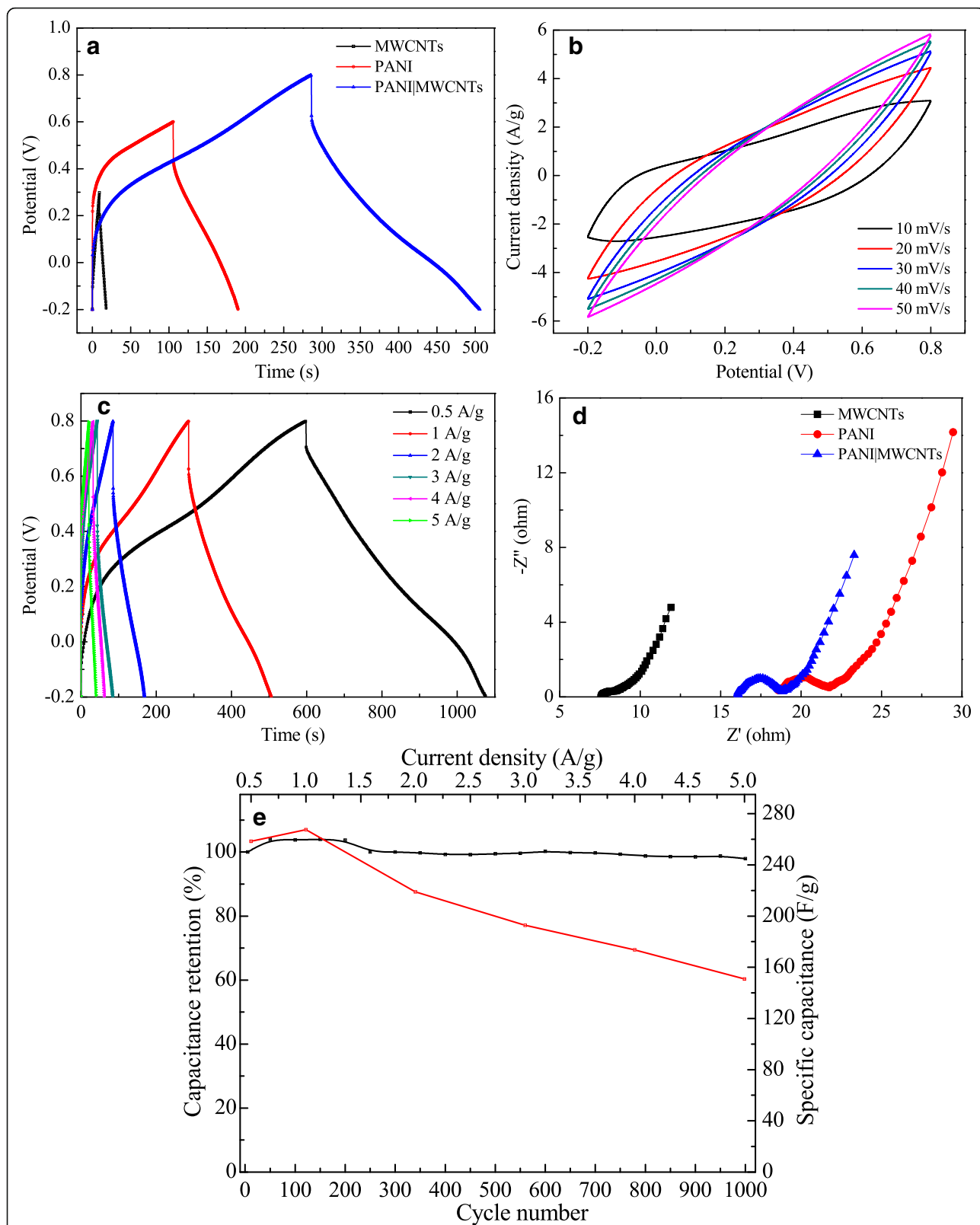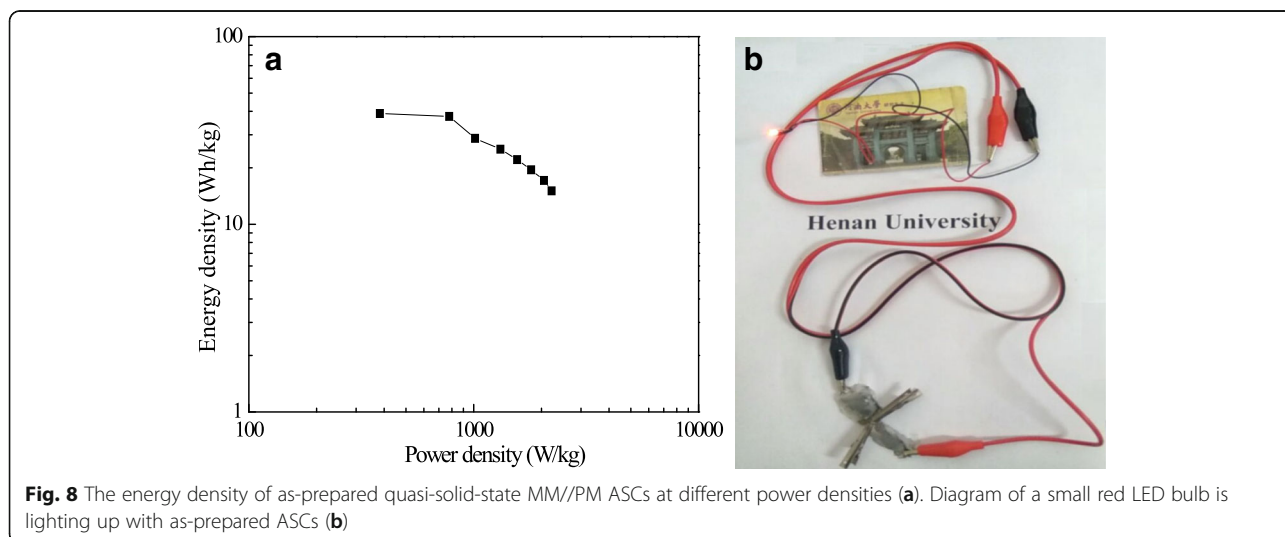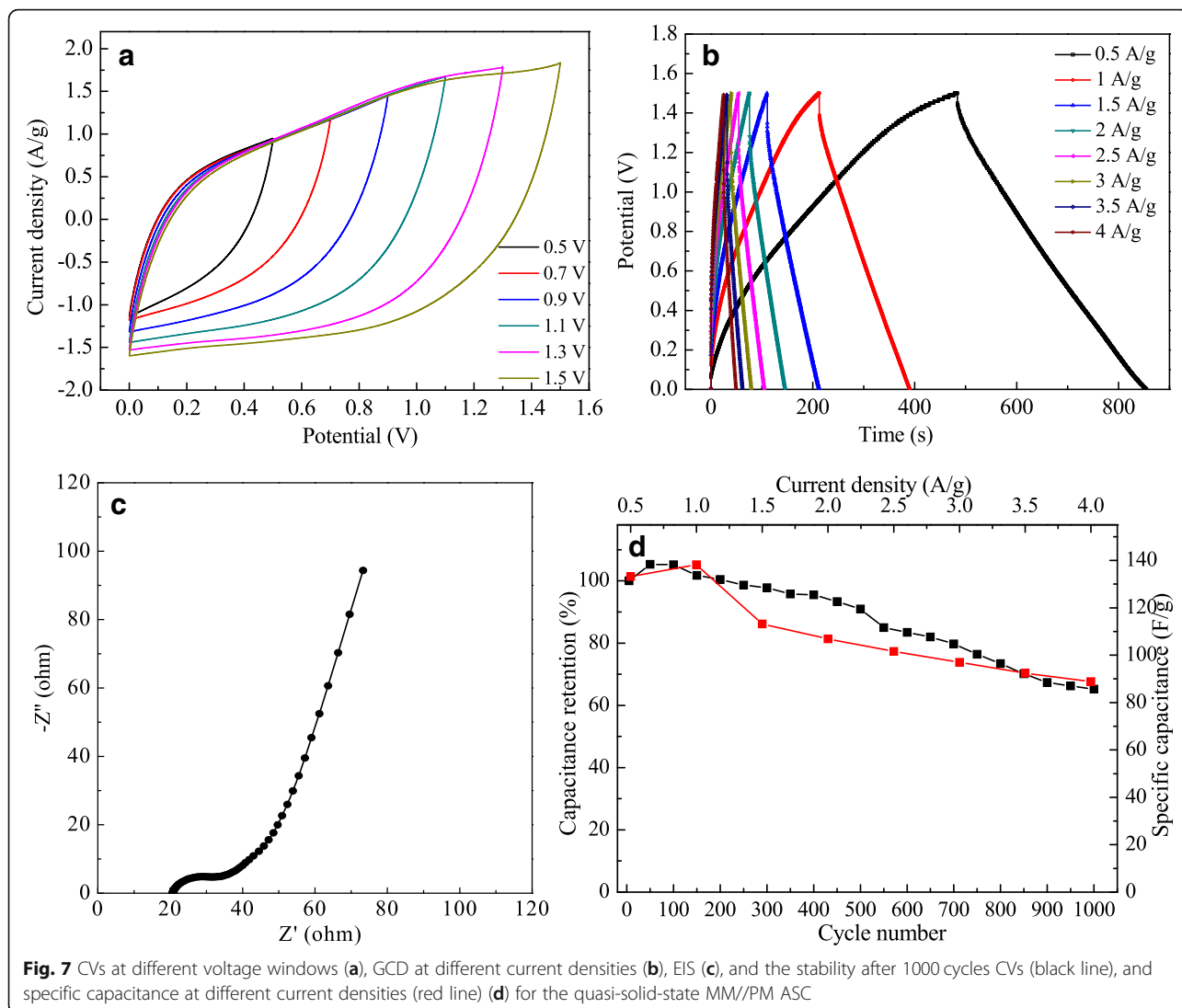
Fig. 6 GCD curves of PANI, MWCNTs, and PANI|MWCNTs electrodes at 1 A/g (**a**); CV curves of PANI|MWCNTs electrode at different scanning speeds (**b**); GCD curves of PANI|MWCNTs electrode at different current densities (**c**); EIS of PANI, MWCNTs, and PANI|MWCNTs electrodes (**d**); the stability after 1000 cycles CVs (black line); and specific capacitance at different current densities (red line) of the PANI|MWCNTs electrode (**e**)

Fig. 7 CVs at different voltage windows (**a**), GCD at different current densities (**b**), EIS (**c**), and the stability after 1000 cycles CVs (black line), and specific capacitance at different current densities (red line) (**d**) for the quasi-solid-state MM//PM ASC

Fig. 8 The energy density of as-prepared quasi-solid-state MM//PM ASCs at different power densities (**a**). Diagram of a small red LED bulb is lighting up with as-prepared ASCs (**b**)

transfer resistance of 15.49 Ω, specific capacitance of 138.1 F/g at 1 A/g and 1.5 V, which energy density can still maintain 15.09 Wh/kg at a power density of 2217.95 W/kg. Two neutral quasi-solid-state MM//PM ASCs connected in series can light a red LED lamp. These results further indicate that this asymmetric supercapacitor has a good application prospect.

Abbreviations
ASC: Asymmetric supercapacitor; Cs: Specific capacitance; CV: Cyclic voltammetry; E: Energy density; EIS: Electrochemical impendence spectroscopy; GCD: Galvanostatic current charge-discharge; MoS_2: Molybdenum disulfide; MWCNTs: Multi-walled carbon nanotubes; PANI: Polyaniline; Rct: Charge transfer resistance; Rct: The charge-transfer resistance; Rs: Solution resistance; SEM: Scanning electron microscopy; η: Power density

Availability of Data and Materials
All datasets on which the conclusions of the manuscript rely are presented in the main paper.

Authors' Contributions
BC carried out the experiments, participated in the sequence alignment, and drafted the manuscript. RC participated in the device preparation. FT, XL, and JH were involved in the SEM, EIS, and CV analysis of the devices. GY was responsible to draft the manuscript. All authors read and approved the final manuscript.

Competing Interests
The authors declare that they have competing interests.

Publisher's Note
Springer Nature remains neutral with regard to jurisdictional claims in published maps and institutional affiliations.

Author details
[1]Henan Key Laboratory of Photovoltaic Materials and Laboratory of Low-Dimensional Materials Science, Henan University, Kaifeng 475004, China. [2]School of Physics and Electronics, Henan University, Kaifeng 475004, China. [3]School of Materials Science and Engineering, Shaanxi University of Science and Technology, Xi'an 710021, China.

References
1. Liu T, Zhang F, Song Y, Li Y (2017) Revitalizing carbon supercapacitor electrodes with hierarchical porous structures. J Mater Chem A 5: 17705–17733
2. Smoukov SK, Fong KD, Wang TS (2017) Multidimensional performance optimization of conducting polymer-based supercapacitor electrodes. Sustainable Energy Fuels 1:1857–1874
3. Chen L-F, Huang Z-H, Liang H-W, Guan Q-F, Yu S-H (2013) Bacterial-cellulosederived carbon nanofiber@MnO_2 and nitrogen-doped carbon nanofiber electrode materials: an asymmetric supercapacitor with high energy and power density. Adv Mater 25:4746–4752
4. Yang C, Shen J, Wang C, Fei H, Bao H, Wang G (2014) All-solid-state asymmetric supercapacitor based on reduced graphene oxide/carbonnanotube and carbon fiber paper/polypyrrole electrodes. J Mater Chem A 2:1458–1464
5. Choudhary N, Li C, Moore J, Nagaiah N, Zhai L, Jung Y, Thomas J (2017) Asymmetric supercapacitor electrodes and devices. Adv Mater 29:1605336
6. Sun G, Zhang X, Lin R, Yang J, Zhang H, Chen P (2015) Hybrid fibers made of molybdenum disulfide, reduced graphene oxide, and multi-walled carbon nanotubes for solid-state, flexible, asymmetric supercapacitors. Angew Chem Int Ed 54:4651–4656
7. Ma W, Chen S, Yang S, Chen W, Weng W, Cheng Y, Zhu M (2017) Flexible all-solidstate asymmetric supercapacitor based on transition metal oxide nanorods/reduced graphene oxide hybrid fibers with high energy density. Carbon 113:151–158
8. Pan S, Ren J, Fang X, Peng H (2016) Integration: an effective strategy to develop multifunctional energy storage devices. Adv Energy Mater 6: 1501867
9. Wu C, Cai JJ, Zhang QB, Zhou X, Zhu Y, Shen PK, Zhang KL (2015) Hierarchical Mesoporous Zinc–Nickel–Cobalt Ternary Oxide Nanowire Arrays on Nickel Foam as High-Performance Electrodes for Supercapacitors. ACS Appl Mater Interfaces 7:26512–26521
10. Kuang M, Zhang YX, Li TT, Li KF, Zhang SM, Li G, Zhang W (2015) Tunable synthesis of hierarchical $NiCo_2O_4$ nanosheets-decorated cu/CuOx nanowires architectures for asymmetric electrochemical capacitors. J Power Sources 283:270–278
11. Qiu KW, Lu M, Luo YS, Du XW (2017) Engineering hierarchical nanotrees with CuCo trunks and NiO branches for high-performance supercapacitors. J Mater Chem A 5:5820–5828
12. Wang T, Le QJ, Zhang GD, Zhu SJ, Guan B, Zhang JM, Xing SX, Zhang YX (2016) Facile preparation and sulfidation analysis for activated multiporous carbon@$NiCo_2S_4$ nanostructure with enhanced supercapacitive properties. Electrochim Acta 211:627–635
13. Ma FX, Yu L, Xu CY, Lou X (2016) Self-supported formation of hierarchical NiCo tetragonal microtubes with enhanced electrochemical properties. Energy Environ Sci 9:862–866
14. Shen LF, Che Q, Li HS, Zhang XG (2014) Mesoporous $NiCo_2O_4$ nanowire arrays grown on carbon textiles as binder-free flexible electrodes for energy storage. Adv Funct Mater 24:2630–2637
15. Kong DZ, Ren WN, Cheng CW, Wang Y, Huang ZX, Yang HY (2015) Three-dimensional $NiCo_2O_4$@Polypyrrole coaxial nanowire arrays on carbon textiles for high-performance flexible asymmetric solid-state supercapacitor. ACS Appl Mater Interfaces 7:21334–21346
16. Wang L, Ma Y, Yang M, Qi Y (2015) Hierarchical hollow MoS_2 nanospheres with enhanced electrochemical properties used as an electrode in supercapacitor. Electrochim Acta 186:391–396
17. Yang X, Niu H, Jiang H, Wang Q, Qu F (2016) A high energy density all-solid-state asymmetric supercapacitor based on MoS_2/graphene nanosheets and MnO_2/graphene hybrid electrodes. J Mater Chem A 4:11264–11275
18. Hu BL, Qin XY, Asiri AM, Alamry KA, Al-Youbi AO, Sun XP (2013) Synthesis of porous tubular C/MoS_2 nanocomposites and their application as a novel electrode material for supercapacitors with excellent cycling stability. Electrochim Acta 100:24–28
19. Ghosh K, Yue CY (2018) Development of 3D MoO_3/graphene aerogel and sandwich-type polyaniline decorated porous MnO_2/graphene hybrid film based high performance all-solid-state asymmetric supercapacitors. Electrochim Acta 276:47–63
20. Zhang HY, Qin G, Lin YX, Zhang DF, Liao HY, Li ZH, Tian JY, Wu QB (2018) A novel flexible electrode with coaxial sandwich structure based polyaniline-coated MoS_2 nanoflakes on activated carbon cloth. Electrochim Acta 264:91–100
21. Tang H, Wang J, Yin H, Zhao H, Wang D, Tang Z (2015) Growth of polypyrrole ultrathin films on MoS_2 monolayers as high-performance supercapacitor electrodes. Adv Mater 27:1117–1123
22. Bhadra S, Khastgir D, Singha NK, Lee JH (2009) Progress in preparation, processing and applications of polyaniline. Prog Polym Sci 34:783–810
23. Zhang K, Zhang LL, Zhao X, Wu J (2010) Graphene/polyaniline nanofiber composites as supercapacitor electrodes. Chem Mater 22:1392–1401
24. Li Y, Zhao X, Xu Q, Zhang Q, Chen D (2011) Facile preparation and enhanced capacitance of polyaniline/sodium alginate nanofiber networks for supercapacitors. Langmuir 27:6458–6463
25. Yan J, Wei T, Shao B, Fan Z, Qian W, Zhang M, Wei F (2010) Preparation of a graphene nanosheet/polyaniline composite with high specific capacitance. Carbon 48:487–493
26. Yan Y, Cheng Q, Zhu Z, Pavlinek V, Saha P, Li C (2013) Controlled synthesis of hierarchical polyaniline nanowires/ordered bimodal mesoporous carbon nanocomposites with high surface area for supercapacitor electrodes. J Power Sources 240:544–550
27. Wang YG, Li HQ, Xia YY (2006) Ordered whiskerlike polyaniline grown on the surface of mesoporous carbon and its electrochemical capacitance performance. Adv Mater 18:2619–2623

28. Li Y, Kang Z, Yan XQ, Cao SY, Li MH, Liu YC, Liu S, Sun YH, Zheng X, Zhang Y (2017) Facile method for preparation of three-dimensional CNT sponge and nanoscale engineering design for high performance fiber-shaped asymmetrical supercapacitors. J Mater Chem A 5:22559–22567

29. Das AK, Bera R, Maitra A, Karan SK, Paria S, Halder L, Si SK, Bera A, Khatua BB (2017) Fabrication of an advanced asymmetric supercapacitor based on a microcubical PB@MnO$_2$ hybrid and PANI/GNP composite with excellent electrochemical behaviour. J Mater Chem A 5:22242–22254

30. Ghosh K, Yue CY, Sk MM, Jena RK (2017) Development of 3D urchin-shaped coaxial manganese dioxide@polyaniline (MnO$_2$@PANI) composite and self-assembled 3D pillared graphene foam for asymmetric all-solid-state flexible supercapacitor application. ACS Appl Mater Interfaces 9:15350–15363

31. Liu A, Zhang HT, Wang G, Zhang JH, Zhang SJ (2018) Sandwich-like NiO/rGO nanoarchitectures for 4 V solid-state asymmetric-supercapacitors with high energy density. Electrochim Acta 283:1401–1410

32. Jiao YZ, Zhang HT, Zhang HL, Liu A, Liu YX, Zhang SJ (2018) Highly bonded T-Nb$_2$O$_5$/rGO nanohybrids for 4 V quasi-solid state asymmetric supercapacitors with improved electrochemical performance. Nano Res 11:4673–4685

33. Ma GF, Peng H, Mu JJ, Huang HH, Zhou XZ, Lei ZQ (2013) In situ intercalative polymerization of pyrrole in graphene analogue of MoS$_2$ as advanced electrode material in supercapacitor. J Power Sources 229:72–78

34. Jiang FR, Li WY, Zou RJ, Liu Q, Xu KB, An L, Hu JQ (2014) MoO$_3$/PANI coaxial heterostructure nanobelts by in situ polymerization for high performance supercapacitors. Nano Energy 7:72–79

35. Andrea L (2018) Flexible supercapacitor electrodes based on MoS$_2$-intercalated rGO membranes on Ti mesh. Mater Sci Semicond Process 73:106–110

36. Fan L-Q, Liu G-J, Zhang C-Y, Wu J-H, Wei Y-L (2015) Facile one-step hydrothermal preparation of molybdenum disulfide/carbon composite for use in supercapacitor. Int J Hydrog Energy 40:10150–10157

37. Yang PH, Mai WJ (2014) Flexible solid-state electrochemical supercapacitors. Nano Energy 8:274–290

38. Yan J, Fan ZJ, Sun W, Ning GQ, Wei T, Zhang Q, Zhang RF, Zhi LJ, Wei F (2012) Advanced asymmetric supercapacitors based on Ni(OH)$_2$/graphene and porous graphene electrodes with high energy density. Adv Funct Mater 22:2632–2641

39. Gao Y-P, Huang K-J, Wu X, Hou Z-Q, Liu Y-Y (2018) MoS$_2$ nanosheets assembling three-dimensional nanospheres for enhanced-performance supercapacitor. J Alloys Compd 741:174–181

40. Huang KJ, Zhang JZ, Shi GW, Liu YM (2014) Hydrothermal synthesis of molybdenum disulfide nanosheets as supercapacitors electrode material. Electrochim Acta 132:397–403

41. Sahatiya P, Jones SS, Badhulika S (2018) 2D MoS$_2$–carbon quantum dot hybrid based large area, flexible UV–vis–NIR photodetector on paper substrate. Appl Mater Today 10:106–114

42. Lee TH, Pham DT, Sahoo R, Seok J, Luu T, Lee YH (2018) High energy density and enhanced stability of asymmetric supercapacitors with mesoporous MnO$_2$@CNT and nanodot MoO$_3$@CNT free-standing films. Energy Storage Mater 12:223–231

43. Li N, Lv T, Yao Y, Li HL, Liu K, Chen T (2017) Compact graphene/MoS$_2$ composite films for highly flexible and stretchableall-solid-state supercapacitors. J Mater Chem A 5:3267–3273

44. Yue GT, Wu JH, Lin J-Y, Xiao YM, Lin JM, Huang ML, Lan Z (2013) A counter electrode of multi-wall carbon nanotubes decorated with tungsten sulfide used in dye-sensitized solar cells. Carbon 55:1–9

45. Yue GT, Wu JH, Xiao YM, Huang ML, Lin JM, Lin J-Y (2013) High performance platinum-free counter electrode of molybdenum sulfide–carbon used in dye-sensitized solar cells. J Mater Chem A 1:1495–1501

46. Ju JG, Zhao HJ, Kang WM, Tian NN, Deng NP, Cheng BW (2017) Designing MnO$_2$ & carbon composite porous nanofiber structure for supercapacitor applications. Electrochim Acta 258:116–123

47. Ruan KB, Hu QC, Wang YZ, Long B, Chen LM, Wu YB (2019) All-solid-state flexible supercapacitors based on sodium copper chlorophyllin with ultra-high rate capability. Mater Let 236:383–386

48. Ghosh A, Lee YH (2012) Carbon-based electrochemical capacitors. ChemSusChem 5:480–499

49. Guo PZ, Gu Y, Lei ZB, Cui YQ, Zhao XS (2012) Preparation of sucrosebased microporous carbons and their application as electrode materials for supercapacitors. Micropor Mesopor Mater 156:176–180

50. Bissett MA, Kinloch IA, Dryfe RA (2015) Characterization of MoS$_2$-graphene composites for high-performance coin cell supercapacitors. ACS Appl Mater Inter 7:17388–17398

51. Nam MS, Patil U, Park B, Sim HB, Jun SC (2016) A binder free synthesis of 1D PANI and 2D MoS$_2$ nanostructured hybrid composite electrodes by the electrophoretic deposition (EPD) method for supercapacitor application. RSC Adv 10:1592–101601

52. Khawula TNY, Raju K, Franklyn PJ, Sigalas I, Ozoemena KI (2016) Symmetric pseudocapacitors based on molybdenum disulfide (MoS$_2$)-modified carbon nanospheres: correlating physicochemistry and synergistic interaction on energy storage. J Mater Chem A 4:6411–6425

53. Ramachandran R, Saranya M, Velmurugan V, Raghupathy BPC, Jeong SK, Grace AN (2015) Effect of reducing agent on graphene synthesis and its influence on charge storage towards supercapacitor applications. Appl Energy 153:22–31

54. Krishnamoorthy K, Veerasubramani GK, Pazhamalai P, Kima SJ (2016) Designing two dimensional nanoarchitectured MoS$_2$ sheets grown on Mo foil as a binder free electrode for supercapacitors. Electrochim Acta 190:305–312

55. Oraon R, Adhikari DA, Tiwari SK, Nayak GC (2016) Nanoclay-based hierarchical interconnected mesoporous CNT/PPy electrode with improved specific capacitance for high performance supercapacitors. Dalton Trans 45:9113–9126

56. Chen M, Dai Y, Wang JJ, Wang Q, Wang YP, Cheng XN, Yan XH (2017) Smart combination of three-dimensional-flower-like MoS$_2$ nanospheres/interconnected carbon nanotubes for application in supercapacitor with enhanced electrochemical performance. J Alloys Compd 696:900–906